E.ON Engineering

E.ON Engineering Limited, Technology Centre, Ratcliffe on Soar, Nottinghamshire, NG11 0EE T +44 (0) 2476 192900 F +44 (0) 115 902 4012 eenukcommunications@eon-engineering.uk,com

UNRESTRICTED

EEN/08/OSP/MA/183/R
Job No: X.A00059
July 2008

ENERGINET.DK PROJECT NUMBER PSO 6520: "CORROSION MEASUREMENTS AT AMV2/AVV2 WITH BIOMASS DUST FIRING"; DONG ENERGY / VATTENFAL: "FIRESIDE CORROSION TESTING WITHIN AMAGER UNIT 2 MARCH 2007"

Prepared for
MR S A JENSEN, DONG ENERGY
by
C. Davis

SUMMARY

Biomass dust firing represents a considerable risk in terms of fireside corrosion and fouling of furnace and superheater / reheater tubing in utility boilers operating at high temperatures and pressures. In order to examine the corrosion rates in a wood / straw fired boiler a pair of fireside corrosion probes were exposed within the Amager Unit 2 boiler. The probes utilised a range of alloys either already present in the boiler, or that were potential candidates for replacement tubing. The measured metal losses and associated wastage rates have been assessed with the conclusions from the test work summarised in this report.

Funding was provided under project PSO 6520 "Corrosion Measurements at AMV2/AVV2 With Biomass Dust Firing". Originally the remainder of the funding was provided by ENERGI E2, but after the creation of DONG Energy and Vattenfall (Denmark), both companies have contributed to project funding.

Prepared by **Approved for publication**

Master copy signed by C J Davis & L W Pinder (23/7/08)

C. J. Davis
Materials

L. W. Pinder
Technical Head, Materials

CONCLUSIONS

1. Corrosion of the various specimens can generally be characterised according to the type of material. The low alloy ferritic specimens suffered general metal loss and enhanced grain boundary attack, forming duplex, but defective corrosion scales. The formation of a dark phase / scale at the metal / scale interface was associated with locally enhanced wastage and was attributed to the presence of chlorine. The martensitic steels suffered uniform wastage and slight subsurface attack with the growth of dense duplex corrosion scales. Occasional dark phase scale was again associated with locally enhanced wastage. The austenitic stainless steels generally suffered slight general and grain boundary attack, again forming dense duplex scales. Only the nickel based weld overlay formed a chromia scale, although it to suffered isolated, irregular breakdown to form duplex scales with slight sub-surface attack.

2. The austentitic material Sanicro25 suffered considerably greater wastage than the other austenitic materials despite higher chromium content. This manifested as subsurface attack within metal grains, and grain boundary penetration, leading to surface metal exfoliation.

3. The specimens exposed at higher temperatures showed greater tendency for corrosion scale and ash interaction, losing chromium into the outer scale and ash, with low levels of ash derived elements in the inner corrosion scales.

4. The defective and hence un-protective nature of the corrosion scales formed by the ferritic specimens suggests that para-linear or linear corrosion kinetics would likely apply to these materials, with corrosion rates remaining high even after extended exposure periods.

5. With the formation of dense duplex corrosion scales by the higher alloy materials, it would be most likely that corrosion rates would follow parabolic rather than linear kinetics, although rates would likely remain higher than would be the case without corrosion scale and ash interaction.

6. With the exception of the copper containing Sanicro25 material, the higher alloy materials containing greater chromium contents performed better than the lower alloy materials, despite increased exposure temperatures. Questions remain as to the performance of copper containing austenitic materials particularly in aggressive biomass derived combustion environments, and as such, Sanicro25 would not be recommended in this application.

7. The dense, predominantly potassium sulphate ash deposits would be considered aggressive at metal temperatures in excess of approximately 560°C, above which molten salt attack would be likely, although the ash would be significantly more aggressive had it contained greater quantities of potassium chloride.

8. In comparison with the probe exposures conducted in the wood and straw fired Amager boiler, the Avedore specimens generally exhibited lower wastage rates, although the rates

measured following the first exposure with the highest percentage wood content were greater and similar to those measured after exposure in Amager.

9. In comparison with the probe exposures conducted at pilot scale, the Amager wastage rates were slightly lower than those measured after exposure to the softwood fuels, and substantially lower than those measured after exposure to the straw and hardwood fuels.

UNRESTRICTED

This report was prepared by E.ON Engineering for DONG Energy.

Telephone +44 (0) 2476 192717
Fax +44 (0) 115 902 4001
E-mail eenukcommunications@eon-engineering-uk.com

CLIENT DISTRIBUTION LIST

EF	Mr S A Jenson	Dong Energy

CONTENTS

Page

1 INTRODUCTION

Between November 2004 and April 2005, a series of pilot scale fireside corrosion probe exposures were conducted in the $1MW_{Thermal}$ Combustion Test Facility located at Power Technology. The research programme was jointly funded by ENERGI E2 and the Elkraft System, Project Number FU2203, "BIOMASS DUST FIRING" [1]. Subsequently, a series of short to medium term corrosion probe exposures has been completed within Avedore Unit 2 and Amager Unit 2 boilers, again whilst burning a range of biomass fuels either alone, or in combination with other fuels such as oil or gas. The tests conducted during March 2007 in the Amager boiler are reported in this document, whilst the tests conducted in Avedore boiler are reported separately [2].

2 TESTING, POST EXPOSURE EXAMINATION AND MEASUREMENT

A single batch of two superheater corrosion probes were exposed within the Amager Unit 2 boiler between 13th March and 31st March 2007, when the heating season finished and the boiler was shut down. During the exposure period the boiler was nominally operating at 2/3 of its rated capacity. These probes have been identified as SHTR95 and SHTR96 and form Batch 4 in this series of tests. Exposure locations within the boiler were determined by availability of access ports in suitable positions. Probe SHTR95 was exposed in the boiler second pass at the 42.6m level, 5.5m from the furnace front wall and 1.0m from the nearest soot blower, above the top horizontal tube bank. Probe SHTR96 was located in the first pass of the boiler at the 38.9m level, 3.1m from the furnace front wall and 0.7m from the nearest soot blower, in the keyhole of the rear most platen superheater (Figure 1). Routine soot blowing continued during the corrosion probe exposures. No attempt was made to measure the flue gas temperatures at the probe exposure locations.

The fuels combusted during the corrosion probe exposures were not analysed and hence the composition was unknown. However, the fuel diet was reported to comprise 63.81%$_{mass}$ wood dust pellets and 36.16%$_{mass}$ straw. The remainder 0.03%$_{tmass}$ heat input comprised heavy fuel oil (7 tonnes) which was utilised within a single day. The fuels were not blended during the exposure, rather the wood and straw fuels were fired separately.

All of the control and logging equipment was installed by DONG energy engineers, who also conducted the exposure of the two superheater type corrosion probes. After removal from the boiler and allowing to cool, the test specimens were given a protective coating of cold curing polyester resin, prior to return to Power Technology for laboratory examination.

A PC based data logging system was utilised that employed Isolated Measurement Pods (IMPs) to monitor the probe metal temperatures. The IMPS were located close to the corrosion probes, with the data returned to the logger using a single sheathed pair of cables. Unfortunately, the data logger suffered a failure during the exposure resulting in the loss of some temperature data. During the periods of missing data, it was known that the boiler remained in operation, and as such it remained possible to determine the total exposure periods and estimate sample temperatures.

2.1 Probe Technology

The probes were of the same design as that previously employed whilst fireside corrosion testing at pilot scale, with the exception of longer carrier tubes to permit access through the power station boiler wall [1]. The superheater probe bodies were approximately 2m in length, permitting the samples to be exposed a minimum of 1m from the furnace wall.

Each corrosion probe carried 10 individual corrosion coupons, which comprised various typical boiler tube materials and a weld overlay (Figure 2). These were exposed to a range of metal temperatures and furnace environments as determined by location in the furnace. Cooling air was introduced through the centre tube to the end sample and passed along the internal surface of the samples before exhausting external to the boiler. The cooling air was heated as it traversed the samples, resulting in a temperature gradient along the length of the probe.

A broad range of alloy materials were utilised which represented the existing materials employed in Amager Unit 2 and alternative alloys that might find application in retrofitting existing stages or in the construction of new biomass fired boilers. This latter group of alternative materials included X10CrMoVNb9-1 (T91), TP347HFG, Sanicro25 and IN625 weld overlay. The material nominal compositions, together with alternate designations, can be found in Table 1. The materials used to manufacture the specimens were standard boiler tube stock / weld overlays and all of the exposed specimens were manufactured with a surface ground, 0.4Ra finish.

The specimens exposed, together with the individual exposure times and calculated surface metal temperatures, are shown in Tables 2. The probe exposure temperatures can also be seen in Figures 3 – 4. Operating temperatures were estimated for the latter part of the exposure according to boiler load after failure of the data logging system.

2.2 Metal Loss and Wastage Rates

The relatively short duration of the exposures requires that very accurate measurements of the metal loss be obtained in order to be able to discern differences in losses between specimens. Traditional methods of measuring the change in thickness of coupon samples after corrosion exposure, such as micrometer or weight loss measurements, do not posses the required accuracy and can not measure the extent of any internal attack. Further, utilisation of these methods would have resulted in the destruction of the corrosion and ash scales, preventing their characterisation. Accordingly, metal losses were measured on polished metallographic cross sections using a digital image analysis technique, developed previously under a Powergen / EPRI Tailored Collaboration Programme, in which the corrosion scales and ash layers were retained [3].

Upon receipt at Power Technology, the corrosion probes were dismantled and the specimens mounted in cold curing epoxy resin. Once cured, the samples were sectioned perpendicular to their exposed and corroded surfaces, before grinding and polishing to a 1μm finish. Non-aqueous lubricants were used at all stages of specimen preparation, in order to prevent the loss of water soluble corrosion products and ash species.

Metal loss measurement for the cylindrical superheater type specimens were determined at up to 48 positions spaced 7.5° apart around the specimen circumference. Without an original surface

reference, the preferred measurement technique determines surface recession by measurement of the internal corrosion scale thickness. Total corrosive attack is determined by the addition of any grain boundary or internal attack. Measurement of the internal scale thickness enables a measurement accuracy of ± 1μm. Where the corrosion scales spalled, metal loss determination falls back on the measurement of the specimen wall thickness, again by digital image analysis, and comparing this measurement with an original wall thickness made prior to exposure using a coordinate measurement machine. The latter technique possesses an accuracy of approximately ± 10μm.

The measured metal losses, together with the corresponding calculated wastage rates are shown in Tables 2. Mean parabolic wastage rates are further shown in Figure 5.

2.3 Ash and Corrosion Scale Characterisation

The retained corrosion scales and ash deposits on each of the specimens were characterised by optical microscopy (Tables 3, 4). Selected specimens were further examined using Scanning Electron Microscopy (SEM), coupled with energy dispersive X-ray spectroscopic analysis (EDS). Back scatter electron images of those samples examined in the SEM are shown in Figures 6 - 11. The elemental composition as determined by EDS of the various phases identified in the SEM, are presented in Tables 5 – 9. Note that, where no values are reported, the particular element was absent or below the limits of detection (approximately 0.2%). Associated with each table is a list of phases present as implied by the EDS analyses.

3 DISCUSSION

3.1 Alloy Composition

A wide range of alloy materials were employed in the corrosion probe exposures. These covered the normal range of chromium contents expected to be found in boiler tubing, with the 13CrMo44 material being the lowest specification alloy containing approximately 1% chromium and Sanicro25 being the highest alloy grade containing approximately 22% chromium. With increasing chromium expected to provide the greatest improvement in corrosion resistance, a wide range in corrosion performance could be expected for the selected materials. The nickel based weld overlay IN625 would also be expected to perform well with a very good corrosion resistance due to its very low iron content.

Whilst chromium would be expected to have the greatest influence on corrosion resistance, other alloying additions made to improve creep rupture strength may have positive or negative effects. For example, copper additions have been associated with a decrease in corrosion performance in some aggressive environments [2]. Dependant upon the combustion environment, increasing chromium content does not always guarantee improved corrosion resistance. Biomass boilers in particular can operate with extremely aggressive, chloride rich, combustion environments. Where chloride ash deposits are found it is often the case that high chromium content austenitic alloys perform relatively badly, with chromium being selectively leached from the tube surface. Where this occurs, the lower chromium content alloys such as the martensitic X20CrMoV121, or the austenitic alloy Eshette1250 can offer the greatest corrosion resistance.

Due to the anticipated improvements with increasing alloy content, the lower alloy materials were exposed only to lower metal temperatures, whilst high alloy materials were exposed to the higher metal temperatures. Whilst this strategy mirrors the material selection process in actual boiler design, it has rendered difficult the assessment of the effect of changes in metal temperature on the corrosion process.

The test materials used during the project can be divided in to four broad groupings:

- Low Alloy Ferritic Steels
- Martensitic Stainless Steels
- Austenitic Stainless Steels
- Nickel (weld overlay) Based Alloy

Regardless of the exposure location within the boiler, the type of corrosive attack suffered by each of these material groups, with one exception (Sanicro25, see below), can be summarised as follows:

The low alloy ferritic steels (1 – 2% chromium) exposed at relatively low metal temperatures, exhibited irregular general wastage, together with enhanced grain boundary attack that extended to a depth of a few metal grains in advance of the solid corrosion scales. Duplex corrosion scales were formed, although in many locations these were defective or laminated and exhibited some sulphide growth. The hotter ferritic samples also exhibited indications of scale and ash interaction / fluxing, with outer scale material being lost into the overlying dense, mixed, particulate and amorphous ash deposit. In addition, indications of a more defective / weaker, darker grey scale phase were found at the interface between the metal and the inner spinel scale. The occurrence of dark phase material was frequently associated with enhanced local wastage. Experience gained from other plant and pilot scale exposures would suggest that dark phase scales at the metal surface are most frequently associated with the presence of chlorine.

The martensitic stainless steels (9 – 12% chromium) were exposed to hotter metal temperatures than the ferritic materials. All of the samples exhibited thin, dense, duplex corrosion scales to their entire surfaces resulting from general, uniform wastage. Most of the samples also exhibited areas of shallow, subsurface attack, leaving the wastage front with a feathered edge (Figure 8). As with the ferritic materials, occasional areas of darker phase scales were noted at the metal / scale interface, with these associated with slightly enhanced attack. Despite exposure at higher temperatures than the ferritic materials, there was only minimal evidence of scale fluxing by the dense overlying, mixed particulate and amorphous ash deposit. The relatively aggressive nature of the environment encountered in the Amager boiler was indicated by the inclusion trace levels of potassium and chlorine within the inner corrosion scales, together with the finding of chromium leached from the inner scale into the outer corrosion scale and at low levels in the ash deposit (Tables 7).

The austenitic stainless steels (15% or more chromium) were exposed at the highest metal temperatures. With the exception of the Sanicro25 material, these specimens also exhibited thin, duplex, predominantly oxide corrosion scales after suffering slight, uniform wastage. Unlike the lower alloys steels, these showed no indication of dark phase scale formation at the metal surface, and in general, exhibited negligible or, only minor, subsurface / grain boundary attack (Figure 6 & 11). With only thin outer corrosion scales formed there were only minor indications

of outer scale and ash interaction / fluxing, although as with the martensitic materials, x-ray analysis indicated the penetration of potassium and chlorine into the inner corrosion scales and loss of chromium from the inner scales into the outer scale and ash deposits (Tables 5 & 9). The occurrence of any measurable or significant corrosion damage after exposures of only a few hundred hours demonstrates the corrosive nature of the combustion environment with the fuels burnt. Ordinarily, in less corrosive environments, such as coal fired boilers, it would not be expected to find breakdown of the initially chromia scales after such short periods. Indeed, an initiation period of several thousand hours is normal before any significant corrosion would be identified.

In contrast to the other austenitic alloys (Eshette1250 and TP347HFG), the Sanicro25 material exhibited a substantially lower corrosion resistance. This was despite a similar chromium content and higher nickel content than the TP347HFG material. It was thought likely that some of the other alloying additions in Sanicro25, in particular copper, included to provide greater creep strength, rendered this particular alloy more vulnerable to attack in the particularly aggressive combustion environment were chlorides were deposited within the ash. Indeed, high levels of chloride were identified in the subsurface attack and inner corrosion scales present on these samples, Table 8. In addition to the thin, duplex scales identified on the other austenitic samples, a considerable proportion of the specimens surface exhibited a sponge like appearance, with the attack having cut holes through the material to depths of several grains (Figures 9 & 10). In this region, EDS indicated the material to have lost a large proportion of the chromium (selectively leached) from the alloy, together with some iron and copper, leaving the remaining porous metal relatively rich in terms of nickel content. Where this occurred the specimen suffered little or no surface recession, but did exhibit the growth of an external corrosion scale. In addition, attack of the grain boundaries left a surface layer where metal grains were lost / exfoliated. This was often accompanied by the formation of a fractured / mechanically weak, dark phase, chloride rich, corrosion scale.

The nickel based weld overlay material IN625 frequently finds application in aggressive boiler environments, such as chloride rich, waste or biomass boilers, where its high nickel and molybdenum contents and low iron content give rise to excellent corrosion resistance. The IN625 was the only material that formed extended areas of extremely thin but protective chromia scale, although it too suffered from slight irregular, general attack, together with slight subsurface oxidation (Figure 7). The outer scale formed was very thin and in close contact with the overlying dense, amorphous ash deposit. Whilst there was no visible scale and ash interaction , potassium and chlorine were detected in the inner corrosion scales and chromium was also detected in the overlying ash deposit (Table 6).

The general observed trends as a function of alloy material and exposure temperatures are summarised in Table 10.

3.2 Metal Losses and Wastage Rates

Duplex corrosion scales would ordinarily be considered protective through the formation of an effective diffusion barrier. As such, it might be expected that parabolic corrosion kinetics would apply, with apparent attack (or linear wastage rates) decreasing with longer exposure periods. However, given the defective and potentially mechanically weak nature of the corrosion scales retained by the ferritic specimens, it would be likely that the scale would not limit diffusion and,

as such, parabolic kinetics would not be fully realised in this case. Instead, it would be likely that greater, paralinear (with repeated removal of a weak scale) or even linear kinetics would apply, with wastage rates remaining high rather than reducing with time. At the temperatures examined, even the linear wastage rates, whilst high, would be considered tolerable.

The dense duplex scales retained by the higher alloy martensitic and austenitic specimens would suggest that parabolic kinetics would be more likely to apply for this class of materials. Table 2 presents the metal loss measurements, together with both the linear and parabolic wastage rates.

Parabolic wastage rates were determined according to the following equation:

$$K = M^2 / T$$

Where K = the parabolic wastage rate constant at a given temperature expressed as $cm^2.s^{-1}$

M^2 = the corrosion loss (total depth of attack) squared expressed as cm^2

T = the exposure period in s

From Table 2 and Figure 5 it can be seen that the measured metal losses and calculated wastage rates were generally greater for the probe SHTR96 that was exposed in the first pass of the boiler. This is consistent with corrosion rates being greater for specimens of the same material exposed at greater temperatures. In addition, SHTR96 was exposed to higher gas temperatures, and hence heat flux, than SHTR95 exposed in the second pass.

Despite the increase in exposure temperature between the ferritic and martensitic alloy specimens, there was a marked decrease in the metal losses for the higher alloy martensitic materials. This reduction in wastage rate would be attributable to the formation of the dense, more protective corrosion scales. Within the martensitic class of materials, the 12% chromium containing X20CrMoV121 also performed significantly better than the 9% chromium containing T91 steel, exhibiting approximately half of the wastage of the 9% chromium steel. Similarly, further reductions in wastage rates were obtained on further increasing the chromium content to 15% (Eshette1250) and 19% (TP347HFG), again despite increasing metal temperatures.

The highest chromium content alloy (Sanicro25) used during these probe exposures suffered much greater wastage than the adjacent TP347HFG samples exposed at similar temperatures, with a unique subsurface / exfoliation mechanism. The SHTR95 Sanicro25 specimen exposed at a mean surface metal temperature of 568°C only exhibited occasional incidences of this severe form of corrosion damage, and as such, the maximum metal loss was substantially greater than the mean loss. The mean loss was similar to that exhibited by the martensitic alloys, although the sample was 15 – 25°C hotter than the martensitic specimens. In contrast, the SHTR96 Sanicro25 specimen, exposed in the first pass of the boiler at a mean surface temperature of 608°C, suffered much more extensive severe corrosion damage, and as such, both the maximum and mean metal losses were much greater than that measured on any of the other specimens. The use of Sanicro25 at high temperature in biomass fuelled boilers with fuels similar to Amager would not be recommended. Such severe attack and internal penetration would imply that the outer scale layer formed was not protective, and that protective, parabolic kinetics would likely not be achieved.

Sanicro25 has a relatively complex composition with a number of minor alloying additions which are used to optimise creep resistance. These include cobalt, tungsten and copper, any one of which may contribute to the relatively poor corrosion performance, although copper has been implicated elsewhere [2].

3.3 Fuel Usage

During the probe exposure period the boiler was either fired with wood or straw pellets with a very small fraction of fuel oil during a single day. Whilst the compositions of the biomass fuels were not determined, the characteristics of the two fuel types can be generalised. Wood fuels have compositions that are typically low in ash (<3%), sulphur (<0.1%), chlorine (<1%) and alkali metals (<15% of ash expressed as alkali oxides), although exceptions do occur, such as Junkers Hardwood, as used in the previous pilot scale studies [1]. As such, wood fuels are relatively benign (unless the material has elevated alkali metal contents). Given the low ash content fouling of heat exchanger (or corrosion probe sample) surfaces does not pose a serious problem.

In contrast straw based fuels have relatively high ash contents (~5%), with greater sulphur (>0.2%), chlorine (>0.2%) and alkali metal (>30% of ash expressed as alkali oxides) [1]. As such straw based fuels have the potential for creating slagging and fouling problems within boilers (and on corrosion probes), with the slag or ash formed being highly aggressive, comprised largely of alkali metal (Na, K) sulphates and chlorides. The combination of 2/3 wood and 1/3 straw based fuels utilised at Amager during the probe exposures could be anticipated to reduce the extent of any slagging, whilst reducing the corrosive effects of firing 100% straw. Despite the blending of the fuels, the corrosion probes still retained substantial deposits of sintered / prior molten ash largely comprising potassium sulphate, with isolated discrete areas of potassium chloride. Such an ash deposit would be considered relatively aggressive with metal temperatures in excess of approximately 560°C were there exists the possibility for molten sulphate formation. However, the ash deposit would be thought much more aggressive if large proportions of alkali chlorides were present, in which case severe or catastrophic wastage rates would have been likely.

Whilst the bulk of the ash deposits comprised potassium sulphate other fuel derived elements were also present. Calcium formed a considerable part of the ash deposit, most probably as calcium sulphate, and which would be considered benign or beneficial through raising the ash melting temperature. Silicon was also present, most probably as inert, particulate, alumino-silicate type mineral matter which would also have been associated other low concentration elements. Other potentially detrimental ash derived elements occasionally detected in trace quantities were zinc, arsenic and lead.

3.4 Comparison of Wastage Rates When Co-Firing Wood, Heavy Fuel Oil and Gas

A parallel corrosion probe study was conducted at Avedore power plant with a number of corrosion probe batches exposed (1, 1b, 2 & 3) whilst firing different blends of wood, fuel oil and gas. The exposures involved a total of five furnace wall type corrosion probes (as previously used at pilot scale) and eight superheater type probes (SHTR84 – SHTR91). Probes were exposed for periods between 33 and 500 hours, from December 2005 to June 2006 [2]. The furnace wall probes each exposed a single specimen low alloy ferritic or martensitic alloy, whilst

the superheater probes utilised a similar material selection to that used at Amager, with the exception that SAVE25 replaced the Sanicro25 alloy. SAVE25 comprises a high alloy austenitic stainless steel similar to Sanicro25, although with slightly higher chromium contents, reduced nickel and tungsten content. It does not contain cobalt, but contains a similar copper content.

The fuels utilised at Avedore were substantially different to that used during the probe exposures in Amager and comprised varying quantities of wood, heavy fuel oil and gas, together with the coal fly ash additive. Average wood blend contents during the probe exposures varied from 52.8%$_{thermal}$ to just 16.3%$_{thermal}$, with the majority of the remainder of the fuel being heavy fuel oil. In addition, variable quantities (2.2 – 6.5 tonnes / hour average) of coal fly ash was injected into the furnace immediately adjacent to the top level burners.

In general, the mean measured parabolic wastage rates for the ferritic materials exposed at Amager were comparable with the high rates observed during the Avedore batch one exposure (SHTR84 – SHTR86). The austentic materials exposed in the second pass at Amager to relatively low metal and gas temperatures / heat fluxes, exhibited wastage rates that were comparable to the lower rates measured in batches two and three from Avedore (SHTR87 – SHTR91). The austenitic materials exposed in the first pass of Amager to higher metal and gas temperatures, exhibited generally higher wastage rates, with the Sanicro25 specimen in particular suffering the greatest rate measured for any of the specimens in either boiler, Figure 12.

All of the martensitic and austenitic specimens exposed in Amager exhibited duplex scales over their entire surfaces. In contrast, the same materials exposed in Avedore frequently exhibited considerable areas essentially undamaged and protected by very thin chromia scales, with only small areas exhibiting localised pitting damage and duplex scale growth. Only the IN625 material exhibited chromia scales after exposure in both boilers.

The ash deposits retained on the corrosion probes from Amager were significantly larger and comprised a solid mass rather than the friable, powdery ash deposits from Avedore. When examined optically and in the SEM the Avedore ash deposits were found to predominantly comprise alumino-silicate, coal fly ash derived particulate material, together with variable quantities of agglomerating ash deposits incorporating potassium and calcium sulphates, iron oxides, magnesium phosphate and barium / titanium oxides.

The performance of the copper containing SAVE25 alloy at Avedore was better than the Sanicro25 alloy exposed at Amager. When exposed to the highest percentage wood fuel content the SAVE25 had inferior corrosion performance compared with the adjacent TP347HFG samples. In contrast, after exposure when firing low percentage of wood fuel the SAVE25 performed significantly better than the TP347HFG. As such, the performance of copper containing alloys may be dependant upon the fuel burnt, with higher percentage biomass being detrimental to their performance.

3.5 Comparison of Pilot and Full Scale Plant Studies

For comparison purposes, Figure 13 shows the mean parabolic wastage rates for the samples previously exposed whilst firing a range of biomass dust fuels after short term, nominally 50 hour exposures in the pilot scale Combustion Test Facility [1]. As with the plant based

exposures, the probes utilised a range of alloy material similar to that used in plant, with the low alloy materials exposed at the lowest temperatures.

Whilst difficult to observe due to the expanded y axis, the data for the Estonian and Canadian softwoods and the Junkers wood blend + additive (DCP) fuels are only slightly higher than that for the highest rates after exposure in Avedore or Amager. In contrast, the pilot scale data for the Junkers Hardwood and straw based fuels were significantly greater than any of the power plant based exposures.

All of the fuels used at pilot scale were burnt with out any oil or gas support, and without any coal fly ash injection. The softwoods had very low ash content and were relatively benign with only very low levels of aggressive alkali metals or chlorides. In contrast the straw and Junkers hardwood contained significantly greater quantities of both alkali metals and chlorides, with these being implicated in the dramatically accelerated wastage.

4 CONCLUSIONS

1. Corrosion of the various specimens can generally be characterised according to the type of material. The low alloy ferritic specimens suffered general metal loss and enhanced grain boundary attack, forming duplex, but defective corrosion scales. The formation of a dark phase / scale at the metal / scale interface was associated with locally enhanced wastage and was attributed to the presence of chlorine. The martensitic steels suffered uniform wastage and slight subsurface attack with the growth of dense duplex corrosion scales. Occasional dark phase scale was again associated with locally enhanced wastage. The austenitic stainless steels generally suffered slight general and grain boundary attack, again forming dense duplex scales. Only the nickel based weld overlay formed a chromia scale, although it to suffered isolated, irregular breakdown to form duplex scales with slight sub-surface attack.

2. The austenitic material Sanicro25 suffered considerably greater wastage than the other austenitic materials despite higher chromium content. This manifested as subsurface attack within metal grains, and grain boundary penetration, leading to surface metal exfoliation.

3. The specimens exposed at higher temperatures showed greater tendency for corrosion scale and ash interaction, losing chromium into the outer scale and ash, with low levels of ash derived elements in the inner corrosion scales.

4. The defective and hence un-protective nature of the corrosion scales formed by the ferritic specimens suggests that para-linear or linear corrosion kinetics would likely apply to these materials with corrosion rates remaining high even after extended exposure periods.

5. With the formation of dense duplex corrosion scales by the higher alloy materials, it would be most likely that corrosion rates would follow parabolic rather than linear kinetics, although rates would likely remain higher than would be the case without corrosion scale and ash interaction.

6. With the exception of the copper containing Sanicro25 material, the higher alloy materials containing greater chromium contents performed better than the lower alloy materials, despite increased exposure temperatures. Questions remain as to the performance of copper containing austenitic materials particularly in aggressive biomass derived combustion environments, and as such, Sanicro25 would not be recommended in this application.

7. The dense, predominantly potassium sulphate ash deposits would be considered aggressive at metal temperatures in excess of approximately 560°C, above which molten salt attack would be likely, although the ash would be significantly more aggressive had it contained greater quantities of potassium chloride.

8. In comparison with the probe exposures conducted in the wood and straw fired Amager boiler, the Avedore specimens generally exhibited lower wastage rates, although the rates measured following the first exposure with the highest percentage wood content were greater and similar to those measured after exposure in Amager.

9. In comparison with the probe exposures conducted at pilot scale, the Amager wastage rates were slightly lower than those measured after exposure to the softwood fuels, and substantially lower than those measured after exposure to the straw and hardwood fuels.

5 REFERENCES

[1] Davis, C. J.; “Elkraft System Project Number FU2203, "Biomass Dust Firing" ENERGI E2: Pilot Scale Studies of the Fireside Corrosion Performance of Furnace Wall and Superheater / Reheater Tube Materials Exposed Whilst Firing Wood or Straw Derived Biomass Fuels”, PT/05/BB909/R, 2005

[2] Davis, C. J.; ENERGINET.DK Project Number PSO 6520: “Corrosion Measurements at AMV2 / AVV2 with Biomass Dust Firing”; DONG ENERGY / VATTENFAL: “FIRESIDE CORROSION TESTING WITHIN AVEDØRE UNIT 2 December 2006 – June 2006”, EEN/08/OSP/MA/184/R.

[3] Davis, C. J., James, P. J., Pinder, L. W.; “Fireside Corrosion in Pulverised-Coal-Fired Boilers: Effect of Coal Chlorine and Combustion Parameters”, EPRI, Palo Alto, CA: 2001. 1001350

Table 1: TEST ALLOYS AND NOMINAL COMPOSITIONS

Alloy	Alternative Designation		Composition (%)											
			C	Si	P	S	V	Cr	Mn	Fe	Ni	Nb	Mo	Others
13CrMo44	1.7335, T11	Min Max	 0.15	 0.15				0.80 1.25	0.30 0.61	 Balance			0.44 0.65	
10CrMo910	1.738, T22	Min Max	0.08 0.14	0.08 0.14	 0.03	0.02 5		2.00 2.50	0.40 0.80	 Balance			0.90 1.10	
X10CrMoVNb9-1	1.4903, T91	Min Max	0.08 0.12	0.08 0.12	 0.02	 0.01	0.18 0.25	8.5 9.5	0.3 0.6	 Balance	0..03 0.07	0.06 0.10	0.85 1.05	N 0.03–0.07, Al 0.04
X20CrMoV12-1 1.4922		 Min Max	 0.17 0.23	 0.17 0.23	 0.03	 0.03	 0.25 0.35	10.0 0 12.5 0	 1	 Balance	 0.30 0.80	 	 0.80 1.20	
Eshette1250		 Min Max	 0.05 0.15	 0.05 0.15	 0.03	 0.03	 0.15 0.40	 14.0 16.0	 5.50 7.00	 Balance	 9.0 12.0	 0.75 1.2	 0.8 1.2	B 0.003–0.009 Ti 0.05
TP347HFG	SA-213 SA-213M	Min Max	0.06 0.10	0.06 0.10	 0.04	 0.03		17.0 20.0	 2	 Balance	9.00 13.0			Nb 8*%C–1.0
Sanicro25 Alloy 174		 Min Max						 22	 0.5	 Balance	 25	 0.4		N 0.2, Co 1.6, Cu 3, W 3.5
IN625 (weld overlay)		Min Max						 21		 5.8	63 (balance)		 8.5	Ti 0.14 Nb+Ta 3.4

Table 2: BATCH FOUR OF SUPERHEATER PROBES EXPOSED 13-31/07/2007, EXPOSURE CONDITIONS, MEASURED METAL LOSSES AND CALCULATED WASTAGE RATES

Probe	Sample	Material	Time At Temperature	Surface Temperature	Measured Metal Loss			Linear Wastage Rate			Parabolic Wastage Rate (*10^{-12})		
					95%ile	Max	Mean	95%ile	Max	Mean	95%ile	Max	Mean
			(Hours)	(°C)	(µm)	(µm)	(µm)	(nmh^{-1})	(nmh^{-1})	(nmh^{-1})	(cm^2s^{-1})	(cm^2s^{-1})	(cm^2s^{-1})
95 (42.6m second pass, south side wall)	1	13CrMo44	442	524	69.9	73.5	34.4	158	166	78	30.7	33.9	7.4
	2	10CrMo910	442	532	85.0	97.2	39.3	192	220	89	45.4	59.4	9.7
	3	T91	442	540	36.9	45.2	11.6	84	102	26	8.6	12.8	0.9
	4	X20CrMoV121	442	547	11.7	12.8	6.7	26	29	15	0.9	1.0	0.3
	5	T91	442	553	16.8	21.2	13.5	38	48	31	1.8	2.8	1.1
	6	E1250	442	559	12.2	16.7	5.1	28	38	12	0.9	1.7	0.2
	7	TP347HFG	442	564	6.2	6.7	2.9	14	15	7	0.2	0.3	0.1
	8	Sanicro25	442	568	32.9	102.8	11.4	74	233	26	6.8	66.4	0.8
	9	TP347HFG	442	571	6.2	8.4	3.4	14	19	8	0.2	0.4	0.1
	10	IN625	442	575	6.9	17.0	3.1	16	38	7	0.3	1.8	0.1
96 (38.9m first pass)	1	13CrMo44	442	511	55.0	60.9	33.7	124	138	76	19.0	23.3	7.1
	2	10CrMo910	442	527	60.2	70.8	34.5	136	160	78	22.8	31.5	7.5
	3	T91	442	542	25.7	35.9	14.6	58	81	33	4.2	8.1	1.3
	4	X20CrMoV121	442	557	13.4	32.2	9.6	30	73	22	1.1	6.5	0.6
	5	T91	442	571	34.4	38.0	20.7	78	86	47	7.4	9.1	2.7
	6	E1250	442	584	31.5	33.5	16.4	71	76	37	6.2	7.0	1.7
	7	TP347HFG	442	596	19.2	31.3	8.5	44	71	19	2.3	6.2	0.5
	8	Sanicro25	442	608	166.2	175.8	96.5	376	398	218	173.5	194.1	58.5
	9	TP347HFG	442	619	38.5	42.4	18.2	87	96	41	9.3	11.3	2.1
	10	IN625	442	643	14.5	15.9	8.0	33	36	18	1.3	1.6	0.4

Table 3: OPTICAL MICROSCOPY CHARACTERISATION OF CORROSION SCALES / ASH DEPOSITS RETAINED ON SUPERHEATER PROBE 95 EXPOSED AT 42.6m IN THE BOILER SECOND PASS, SOUTH SIDE WALL FOR 442 HOURS

Sample Number (Alloy, Temperature °C)	Corrosion Characteristics	Ash Characteristics
1 (13CrMo44, 524)	Duplex oxide scale, frequently defective / spalling and occasionally laminated. Irregular general wastage with shallow grain boundary attack to one or two grains depth.	Agglomeration of particulate material within dense, glassy matrix
2 (10CrMo910, 532)	Predominantly duplex oxide scale with occasional sulphide banding, although spalling and occasionally defective. Outer edge of scale being fluxed by ash deposit with precipitation of oxides within the ash deposit. Attack dominated by grain boundary penetration typically to 2 - 3 grains depth. Inner scale occasionally dark grey coloured, defective / weak.	Agglomeration of particulate material within dense, glassy matrix. Evidence of iron oxide precipitation within glassy phase.
3 (T91, 540)	Mixture of duplex pale grey oxides with slight feather edged subsurface attack and localised more extensive attack associated with penetration of large, dark grey oxides, possibly chloride containing. Occasional sulphide banding and dissolution of scale outer edge into adjacent glassy ash deposit.	Agglomeration of particulate material within dense, glassy matrix. Evidence of iron oxide precipitation within glassy phase.
4 (X20CrMoV121, 547)	Thin duplex oxide scale to entire circumference with minimal sub-surface feather edged attack. Scale virtually all intact and adherent, no indication of defective dark phase at metal surface. No sign of scale dissolution.	Agglomeration of particulate material within dense, glassy matrix
5 (T91, 553)	Thin duplex oxide scale to entire circumference with minimal sub-surface feather edged attack. Scale virtually all intact and adherent, no indication of defective dark phase at metal surface. No sign of scale dissolution.	Agglomeration of particulate material within dense, glassy matrix
6 (E1250, 559)	Thin duplex oxide scale with occasional grain boundary oxidation to a depth of 1 to 2 grains.	Agglomeration of particulate material within dense, glassy matrix
7 (TP347HFG, 564)	Thin duplex oxide scale with negligible subsurface oxidation or grain boundary attack. Uniform wastage	Agglomeration of particulate material within dense, glassy matrix
8 (Sanicro25, 568)	Mixture of attack morphologies: 1. Thin duplex oxides, uniform wastage, 2. Subsurface oxidation at grain boundaries and within grains to give a cloud of dispersed oxides with exfoliation (little surface recession), 3. Thick, defective, dark oxides giving rise to more localised penetration / pitting damage. Some outer scales fluxed and some sulphides present.	Agglomeration of particulate material within dense, glassy matrix. Evidence of iron oxide precipitation within glassy phase.
9 (TP347HFG, 571)	Thin, duplex, predominantly oxide, corrosion scale with minor subsurface / grain boundary attack to a depth of 1 to 2 grains. Generally slight uniform wastage.	Agglomeration of particulate material within dense, glassy matrix. Evidence of iron oxide precipitation within glassy phase.
10 (IN625, 575)	Mixture of slight irregular general attack and attack comprising shallow subsurface oxidation. Attack worst at 3 & 9 o'clock. Some protective chromia	Agglomeration of particulate material within dense, glassy matrix. Thick ash to crown

Table 4: OPTICAL MICROSCOPY CHARACTERISATION OF CORROSION SCALES / ASH DEPOSITS RETAINED ON SUPERHEATER PROBE 96 EXPOSED AT 38.9m IN THE BOILER FIRST PASS FOR 442 HOURS

Sample Number (Alloy, Temperature °C)	Corrosion Characteristics	Ash Characteristics
1 (13CrMo44, 511)	Irregular general wastage with slight grain boundary attack. Defective (laminated), duplex oxide scales with occasional dark phase at metal surface associated with enhanced metal loss	Dense particulate rich deposit within glassy matrix
2 (10CrMo910, 527)	Irregular general wastage with grain boundary attack to a depth of 1 to 2 grains. Predominantly oxide scale with some sulphides present. Some areas of enhanced attack associated with a dark oxide phase at the metal surface. Occasional areas of slight scale fluxing	Dense particulate rich deposit within glassy matrix
3 (T91, 542)	Thin duplex oxide scale to majority of circumference with minimal sub-surface feather edged attack. Scale virtually all intact and adherent. Only occasional indications of defective dark phase at metal surface associated with localised enhanced attack / pitting.	Dense particulate rich deposit within glassy matrix
4 (X20CrMoV121, 557)	Thin duplex oxide scale to entire circumference with minimal sub-surface feather edged attack. Scale virtually all intact and adherent, no indication of defective dark phase at metal surface. No sign of scale dissolution.	Agglomerated particulates within a glassy matrix.
5 (T91, 571)	Duplex predominantly oxide scale containing visible yellow sulphides. Scale predominantly dense but occasionally slightly defective at metal surface. Considerable areas exhibiting sub-surface attack	Agglomerated particulates within a glassy matrix.
6 (E1250, 584)	Thin duplex oxide scale with occasional grain boundary oxidation to a depth of 1 to 2 grains.	Agglomerated particulates within a glassy matrix.
7 (TP347HFG, 596)	Thin duplex oxide scale with negligible subsurface oxidation or grain boundary attack. Uniform wastage	Agglomerated particulates within a glassy matrix.
8 (Sanicro25, 608)	Considerable sub-surface and grain boundary attack leading to exfoliation of metal grains. Original surface remains apparent with negligible recession, but considerable overlying corrosion product (oxide)	Agglomerated particulates within a glassy matrix.
9 (TP347HFG, 619)	Very thin duplex oxide scale with negligible subsurface oxidation or grain boundary attack. Uniform wastage	Agglomerated particulates within a glassy matrix.
10 (IN625, 643)	Mixture of slight irregular general attack and attack comprising shallow subsurface oxidation. Latter leading to occasional slight exfoliation of thin surface layer. Attack worst at 3 and 9 o'clock	Agglomeration of particulate material within dense, glassy matrix.

Table 5: ENERGY DISPERSIVE SPECTROSCOPY (EDS) RESULTS BATCH 4 SUPERHEATER SAMPLE 9507, TP347HFG, EXPOSED SOUTH SIDE WALL IN THE SECOND PASS, 42.6M, AT 564°C FOR 442 HOURS

Material		Atomic percentage																							
		O	Na	Mg	Al	Si	P	S	Cl	K	Ca	Ti	V	Cr	Mn	Fe	Ni	Cu	Zn	As	Nb	Mo	Ba	W	Pb
Amorphous Ash	Max	74.9	0.4	1.1	0.4	3.6	0.7	10.1	1.5	14.3	5.2			1.0	0.2	2.7	0.4		0.4	0.4					
	Min	64.3	0.3			0.8	0.2	5.2	0.3	7.4	1.8			0.2		0.4									
Mixed Outer Scale & Ash	Max	68.1	0.5	1.5		0.7	0.4	0.6		0.9	1.7			4.2	1.4	21.6	1.0				0.8				
	Min	66.1	0.4			0.4		0.3		0.8	0.4			3.5	1.0	21.5	0.7				0.2				
Inner Scale		57.7	0.5		0.7	0.9		0.4	0.2	1.0	0.3			14.5	0.8	17.0	5.4				0.4				

Implied Compounds In Ash: Potassium Sulphate, Calcium Sulphate, Potassium Chloride, Alumino-Silicates

Table 6: EDS RESULTS BATCH 4 SUPERHEATER SAMPLE 9510, IN625, EXPOSED SOUTH SIDE WALL IN THE SECOND PASS, 42.6M, AT 575°C FOR 442 HOURS

Material		Atomic percentage																							
		O	Na	Mg	Al	Si	P	S	Cl	K	Ca	Ti	V	Cr	Mn	Fe	Ni	Cu	Zn	As	Nb	Mo	Ba	W	Pb
General Ash		71.5	0.5	1.1	0.2	4.8	0.7	4.8	2.0	8.4	4.5			0.2		0.8	0.3								
Amorphous Ash	Max	72.5	0.5	1.4	0.3	6.0	1.0	11.5	1.8	13.9	5.4			0.4	0.4	1.0	0.4		0.2						
	Min	65.3	0.3	0.8		0.5	0.4	3.7	0.4	6.4	3.9			0.2		0.7									
Particulate Ash	Max	65.1	0.7	0.6		3.8	0.4	2.6	26.8	26.0	2.9						0.6			0.2	0.5	0.8		0.2	0.5
	Min	43.4	0.7			1.1	0.3		10.8	12.0	1.8														
Mixed Outer Scale & Ash	Max	76.4	0.8	1.1	0.7	1.4	0.2	0.8	0.5	1.5	13.4			4.1	0.2	1.8	26.4				0.9	0.5			
	Min	58.7	0.3	0.8	0.2	0.8	0.2	0.6	0.3	0.7	1.6			1.0		0.9	2.9				0.9	0.5			
Inner Scale	Max	60.1	0.5		0.4	0.3	0.2	0.8	0.6	1.5	1.3	0.3		14.6		2.6	13.5				1.6	1.3			
	Min																								

Implied Compounds In Ash: Potassium Sulphate, Calcium Sulphate, Potassium Chloride, Alumino-Silicates

Table 7: EDS RESULTS BATCH 4 SUPERHEATER SAMPLE 9605, T91, EXPOSED IN THE FIRST PASS, 38.9M, AT 571°C FOR 442 HOURS

Material		Atomic percentage																							
		O	Na	Mg	Al	Si	P	S	Cl	K	Ca	Ti	V	Cr	Mn	Fe	Ni	Cu	Zn	As	Nb	Mo	Ba	W	Pb
General Ash		68.1	0.4	3.0	1.1	4.5	0.9	0.4	2.3	1.9	9.6			0.8	0.5	5.4	0.5		0.2			0.2			
Amorphous Ash	Max	70.8	1.5	2.3	1.0	2.4	0.7	5.7	1.3	14.4	16.2			1.3	0.9	6.3	1.1		0.4						
	Min	66.1	0.3	0.4	0.2	0.9	0.2	0.2	0.4	1.7	1.3			0.4	0.3	3.9									
Mixed Outer Scale & Ash	Max	68.4	1.8	1.9	2.1	5.1	0.5	1.9	4.6	7.7	3.7		0.2	1.7	0.4	35.3	0.9					0.3			
	Min	60.3		0.5	0.3			0.4		0.3	0.2			0.5	0.2	9.1									
Inner Scale	Max	61.8	0.2	0.3	0.3	1.1			0.3	0.4	0.4	0.6	0.2	8.3	0.8	29.6					0.4	0.7	0.2		
	Min	58.1				0.5			0.2	0.3				8.0	0.3	27.8						0.6			

Implied Compounds In Ash: Potassium Sulphate, Calcium Sulphate, Potassium Chloride, Alumino-Silicates, Iron Oxides

Table 8: EDS RESULTS BATCH 4 SUPERHEATER SAMPLE 9608, SANICRO25, EXPOSED IN THE FIRST PASS, 38.9M, AT 608°C FOR 442 HOURS

Material		Atomic percentage																						
		O	Na	Mg	Al	Si	P	S	Cl	K	Ca	Ti	V	Cr	Mn	Fe	Ni	Cu	Zn	As	Nb	Mo	Ba	W	Pb
Amorphous Ash	Max	71.3	1.4	2.2	0.6	8.4	1.2	8.1	2.4	13.6	7.1			2.3	0.7	6.2	1.2	0.6	0.4						
	Min	62.6	0.3	0.6		2.8	0.4	2.6	0.3	3.4	4.1					0.6									
Particulate Ash	Max	70.1	1.3	16.5	11.4	28.8	3.8	8.2	0.3	12.7	13.1	0.7	0.6	2.3	0.2	14.3	0.5	0.2	0.3						0.4
	Min	58.9				2.2		0.2			0.3					0.2									
Mixed Outer Scale & Ash	Max	72.4	0.5	1.7	0.9	2.0	0.5	4.4	1.0	2.6	7.6			18.7	0.8	37.7	0.9	1.9	0.2						
	Min	56.3		0.2		0.5		0.5			0.3			0.4		3.5									
Inner Scale	Max	61.1	0.3	0.3	0.7	1.4		3.1	8.2	1.0	0.2			4.2	0.2	34.6	13.0	1.0			0.3			1.5	
	Min	55.3				0.2								1.6		12.8									
Sub-surface Attack	Max	46.4	0.6	0.4	0.5	0.5	0.2	0.8	3.8	1.1	0.2			7.4	0.2	31.8	33.5	1.4			0.6			1.7	
	Min	23.8						0.2	0.7	0.5				3.8		21.3	20.6	0.8						1.1	

Implied Compounds In Ash: Potassium Sulphate, Calcium Sulphate, Potassium Chloride, Alumino-Silicates, Iron Oxides

Table 9: EDS RESULTS BATCH 4 SUPERHEATER SAMPLE 9609, TP347HFG, EXPOSED IN THE FIRST PASS, 38.9M, AT 619°C FOR 442 HOURS

Material		Atomic percentage																							
		O	Na	Mg	Al	Si	P	S	Cl	K	Ca	Ti	V	Cr	Mn	Fe	Ni	Cu	Zn	As	Nb	Mo	Ba	W	Pb
General Ash		75.3	0.5	0.6	0.4	3.5	0.3	3.6	2.3	7.3	2.5			0.7		2.4	0.4								
Amorphous Ash	Max	61.4	0.6	1.1		0.8	0.3	14.5	0.5	23.0	2.1			0.8	0.2	2.6	0.4								0.3
	Min	58.2	0.3	0.4		0.2		11.3	0.2	18.4	1.1			0.4		1.2									0.3
Particulate Ash	Max	67.3	1.5	1.0	5.3	18.8	0.6	1.3	0.8	6.5	6.1		0.2	3.3	0.5	14.2	3.7		0.3	0.4			0.6		
	Min	63.6			0.9	6.8		0.3	0.3	1.3	1.0			0.2		0.9							0.2		
Mixed Outer Scale & Ash	Max	69.6	0.7	0.7	0.6	2.3		7.4	1.5	12.1	2.1			5.3	0.4	28.4	0.8		0.3	0.7			0.4		
	Min	59.9				0.3		1.2	0.2	1.7	0.3			1.0		3.3	0.5								
Inner Scale	Max	55.0	6.5	0.5		1.1		1.0	1.0	0.4	0.6			16.2		16.0	1.4	0.9			0.8	0.4	0.2	0.3	

Implied Compounds In Ash: Potassium Sulphate, Calcium Sulphate, Potassium Chloride, Alumino-Silicates, Iron Oxides

Table 10: GENERALISED SUMMARY OF TRENDS IN EXPOSURE TEMPERATURES, WASTAGE RATE AND DAMAGE MORPHOLOGY FOR THE MATERIALS EXPOSED IN AMAGER

Alloy	Temperature Exposure Range (°C)	Wastage Rates	Linear / Parabolic	Damage Morphology
13CrMo44	511 - 524	High	(Para-) Linear	General wastage, slight subsurface attack
10CrMo910	527 - 532	High	(Para-) Linear	General wastage with grain boundary attack
T91	540 - 571	Medium	Parabolic	Irregular general wastage, slight subsurface attack
X20CrMoV121	547 - 557	Medium	Parabolic	Irregular general wastage, very slight subsurface attack
Eshette1250	559 - 584	Low	Parabolic	General wastage with grain boundary attack
TP347HFG	564 - 619	Low	Parabolic	General wastage with slight grain boundary attack
Sanicro25	568 - 608	Low	(Para-) Linear	General wastage, subsurface selective corrosion and exfoliation of surface metal grains.
IN625	575 - 643	Low	Parabolic	Mixture of protective chromia with no observable attack and irregular general wastage, with some slight pitting and subsurface damage

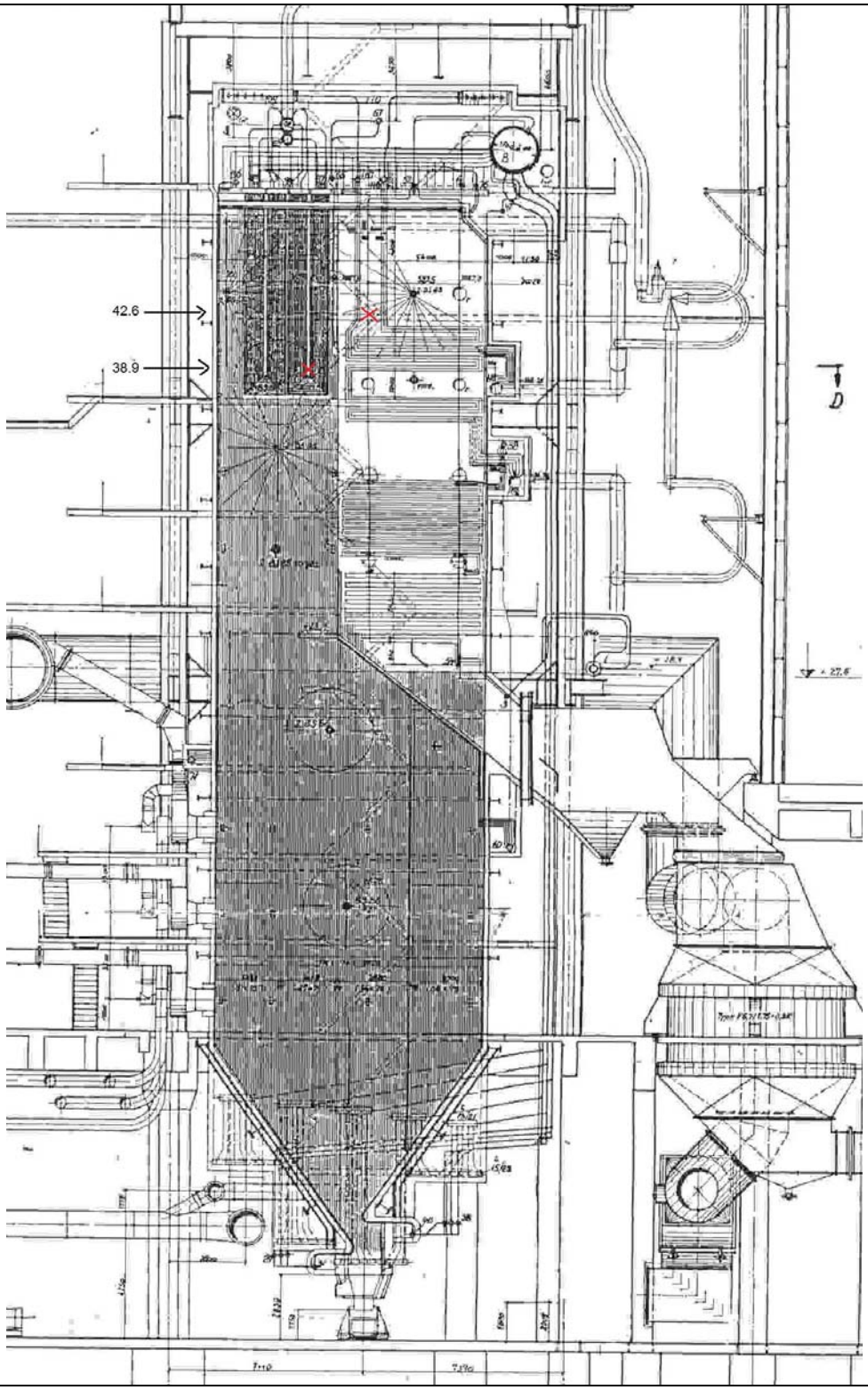

Figure 1: SCHEMATIC DRAWING OF AMAGER UNIT 2 BOILER INDICATING THE POSITION OF THE PROBE EXPOSURE PORTS AT 42.6M AND 38.9M ELEVATIONS

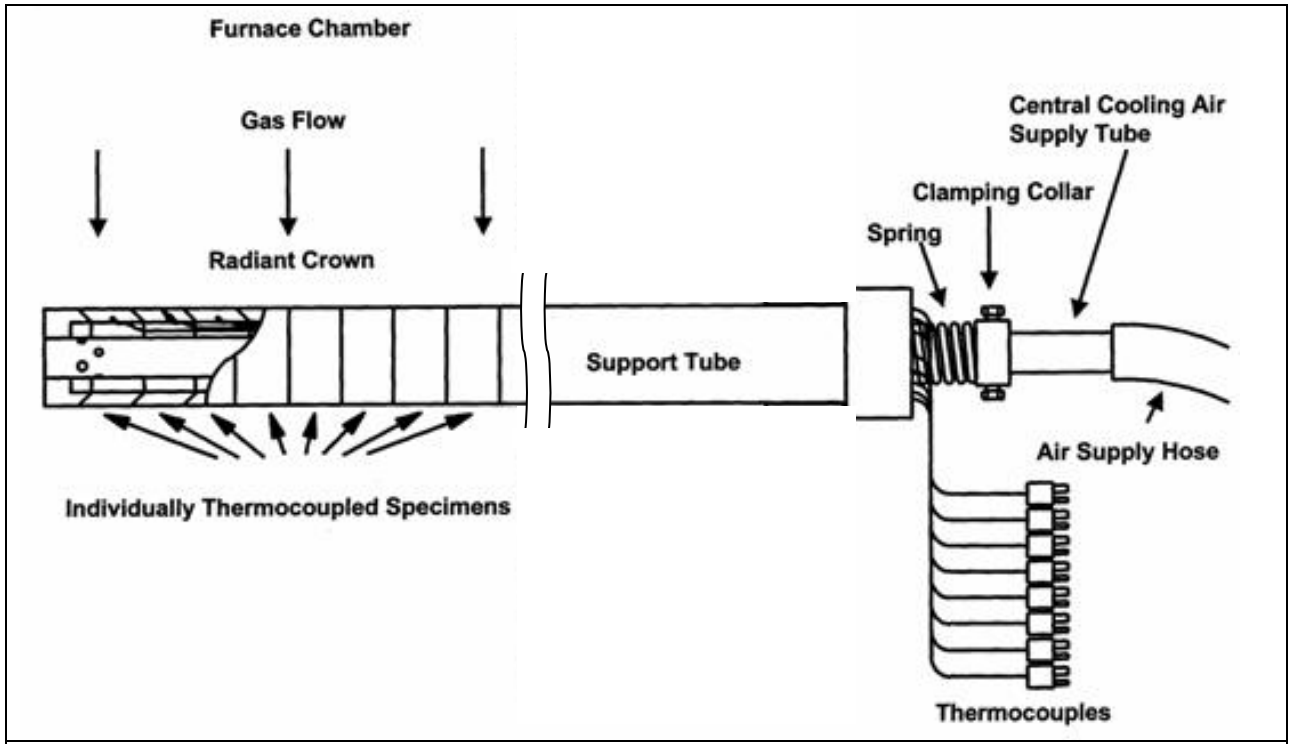

Figure 2: SCHEMATIC DRAWING OF A SUPERHEATER / REHEATER CORROSION PROBE

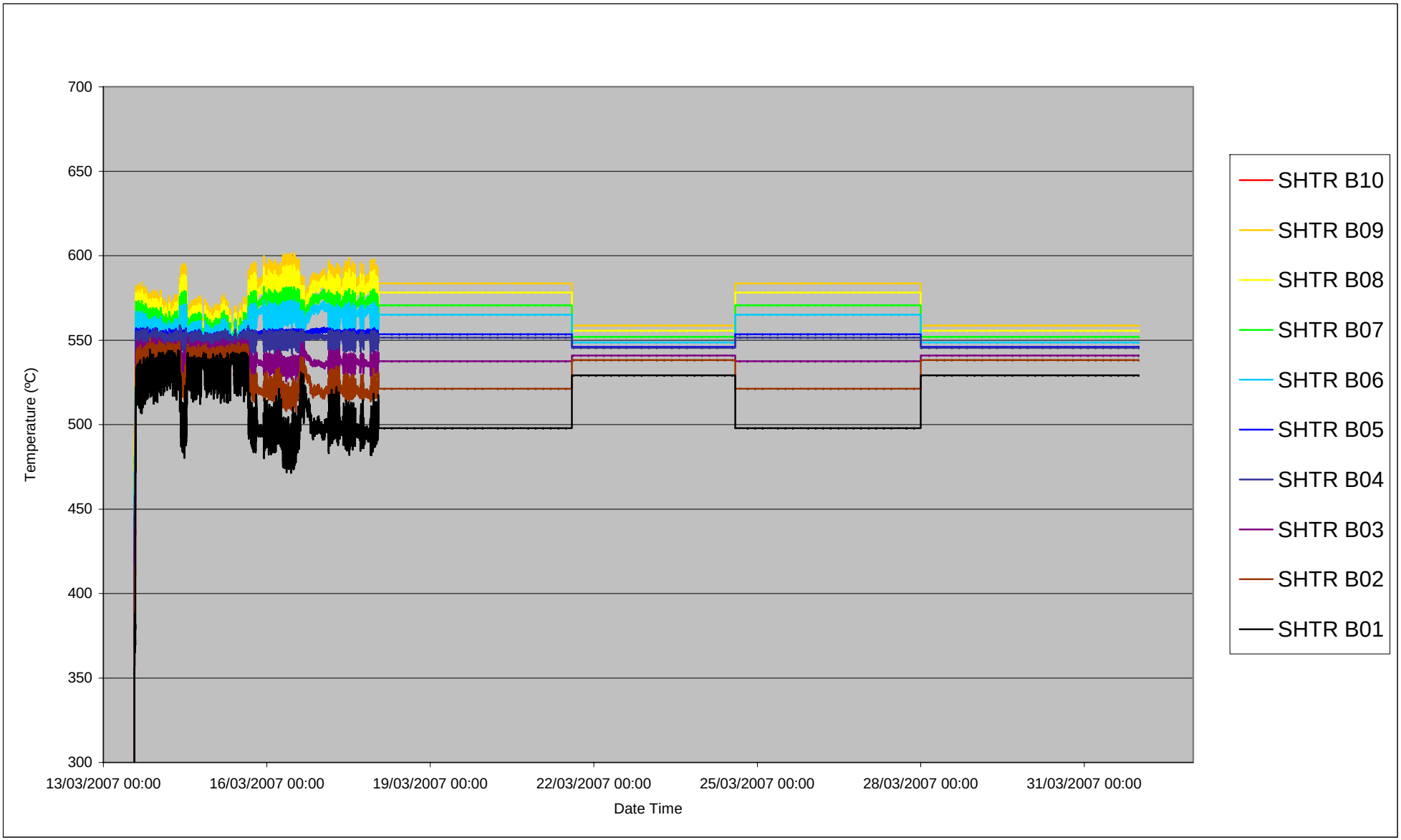

Figure 3: BATCH FOUR PROBE SHTR95 SPECIMEN MEASURED (AND ESTIMATED) TEMPERATURES

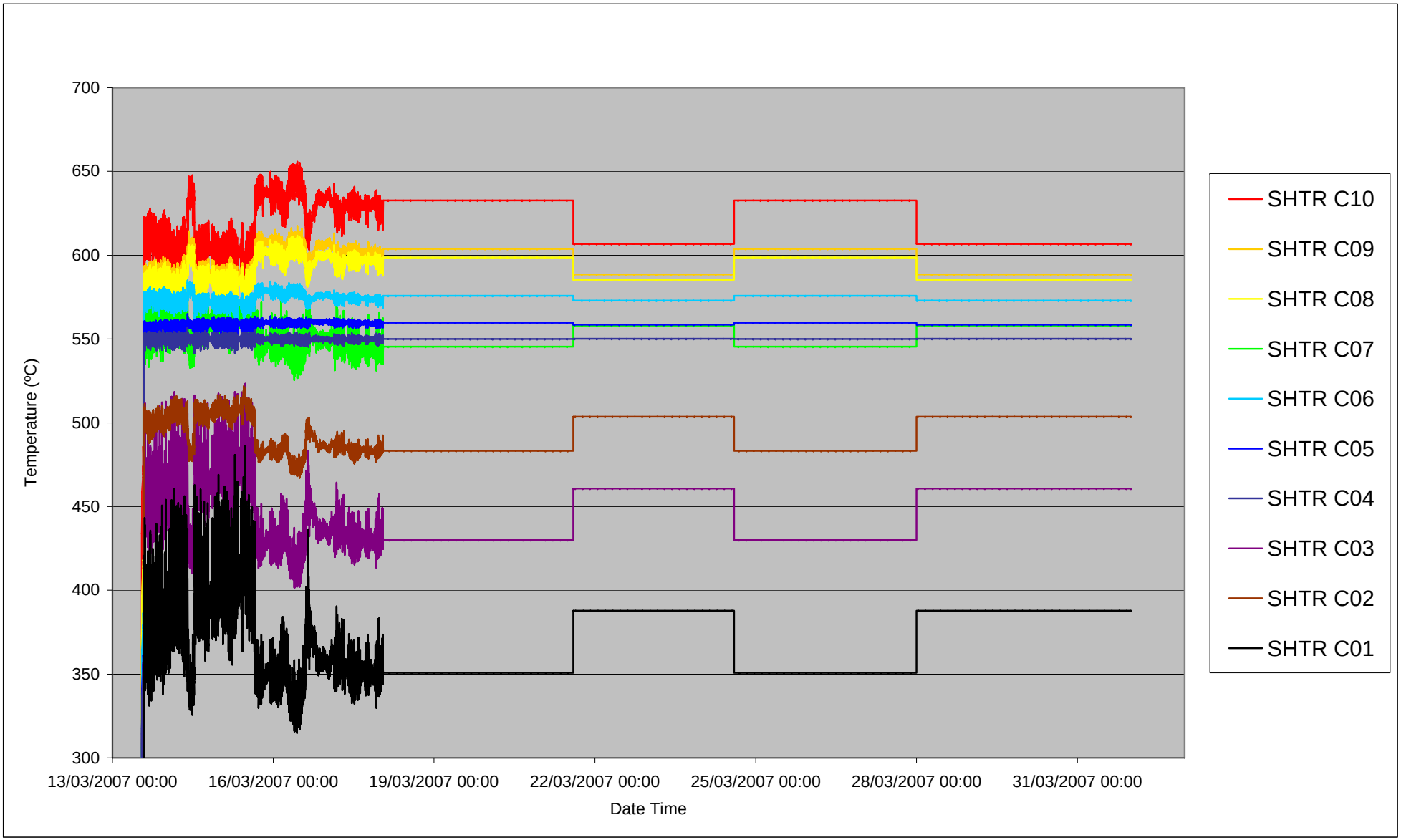

Figure 4: BATCH FOUR PROBE SHTR96 SPECIMEN MEASURED (AND ESTIMATED) TEMPERATURES

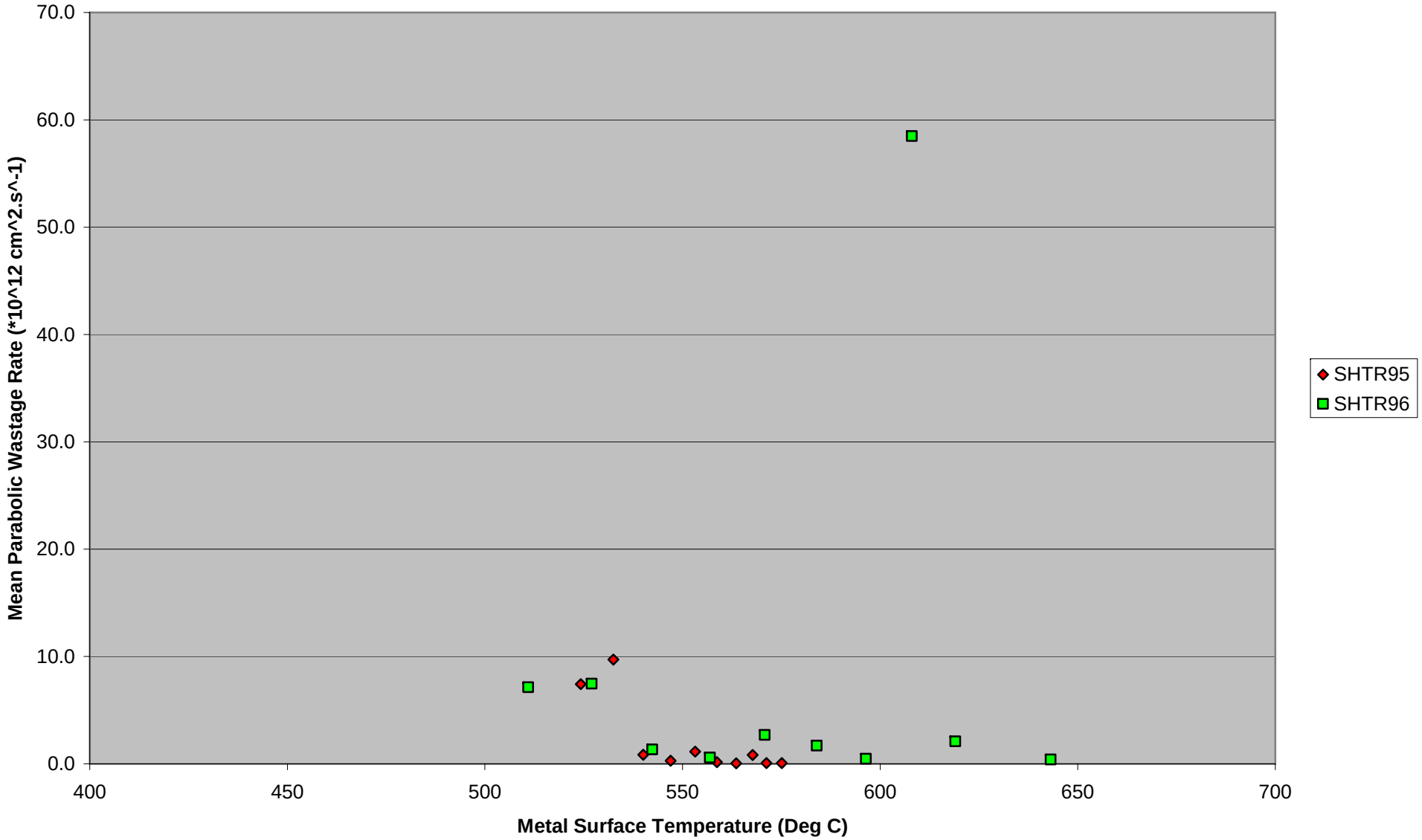

Figure 5: BATCH FOUR: CALCULATED WASTAGE RATES FOR THE SAMPLES EXPOSED IN AMAGER UNIT 2 AFTER 442 HOURS EXPOSURE

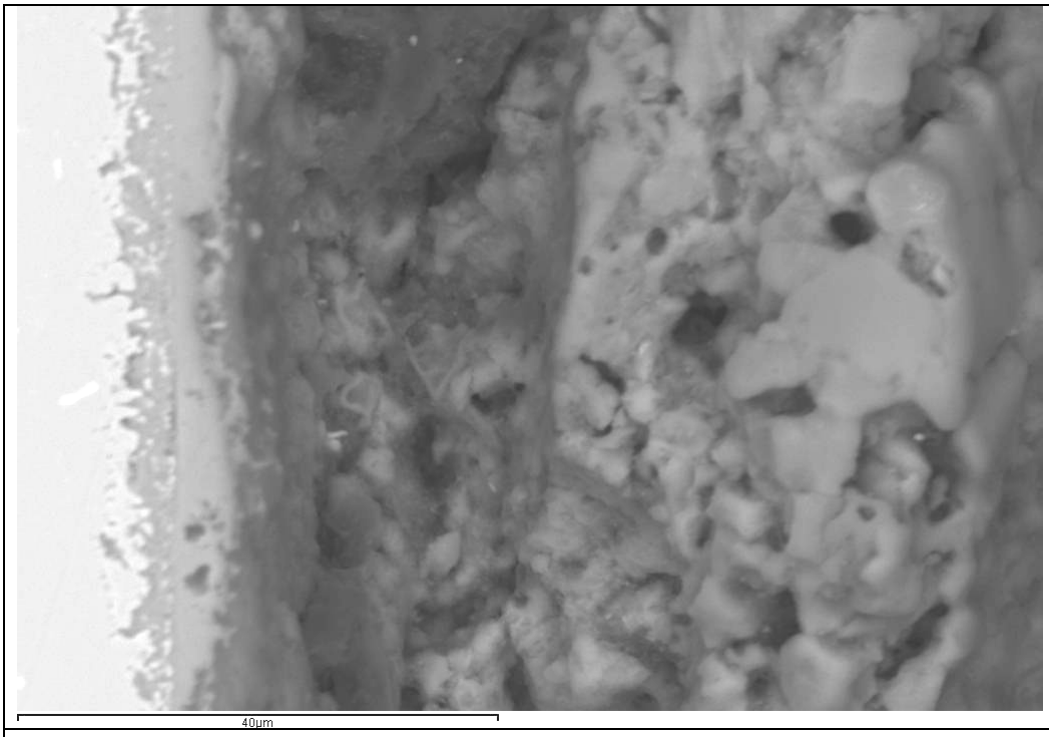

Figure 6: **SHTR95, SPECIMEN 7, TP347HFG, 564°C FOR 442 HOURS, BACK SCATTER ELECTRON IMAGES SHOWING LOCALISED AND SUBSURFACE ATTACK WITH DUPLEX CORROSION SCALES. SCALE OVERLAID BY AN AMORPHOUS ASH DEPOSIT**

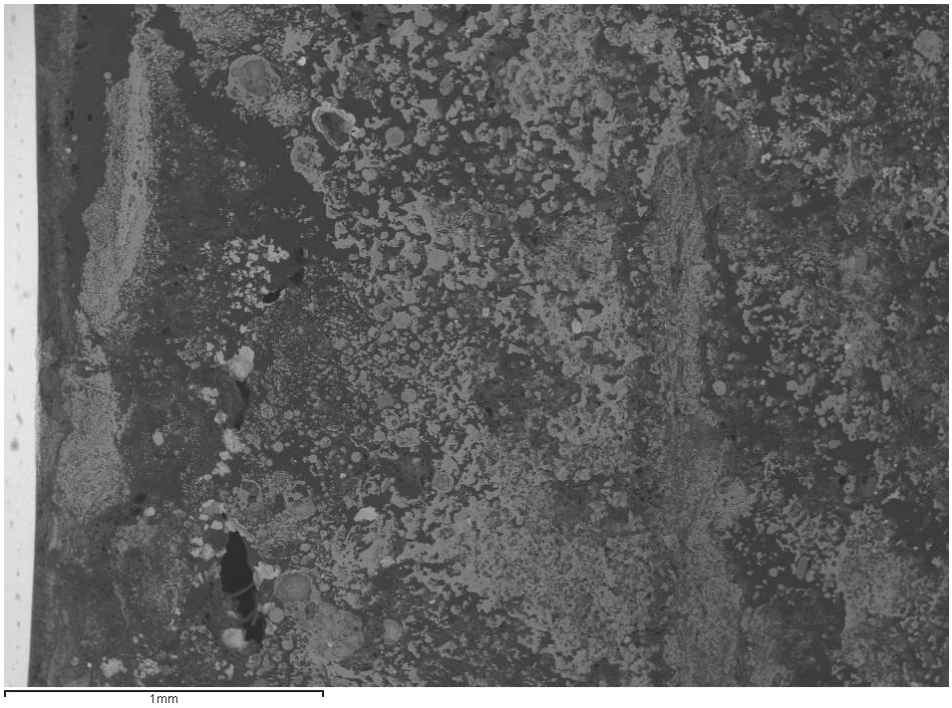

Figure 7: **SHTR95, SPECIMEN 10, IN625, 575°C FOR 442 HOURS, BACK SCATTER ELECTRON IMAGES SHOWING LOCALISED AND SUBSURFACE ATTACK WITH DUPLEX CORROSION SCALES. DEFECTIVE OUTER SCALE MIXED WITH THE AMORPHOUS ASH DEPOSIT**

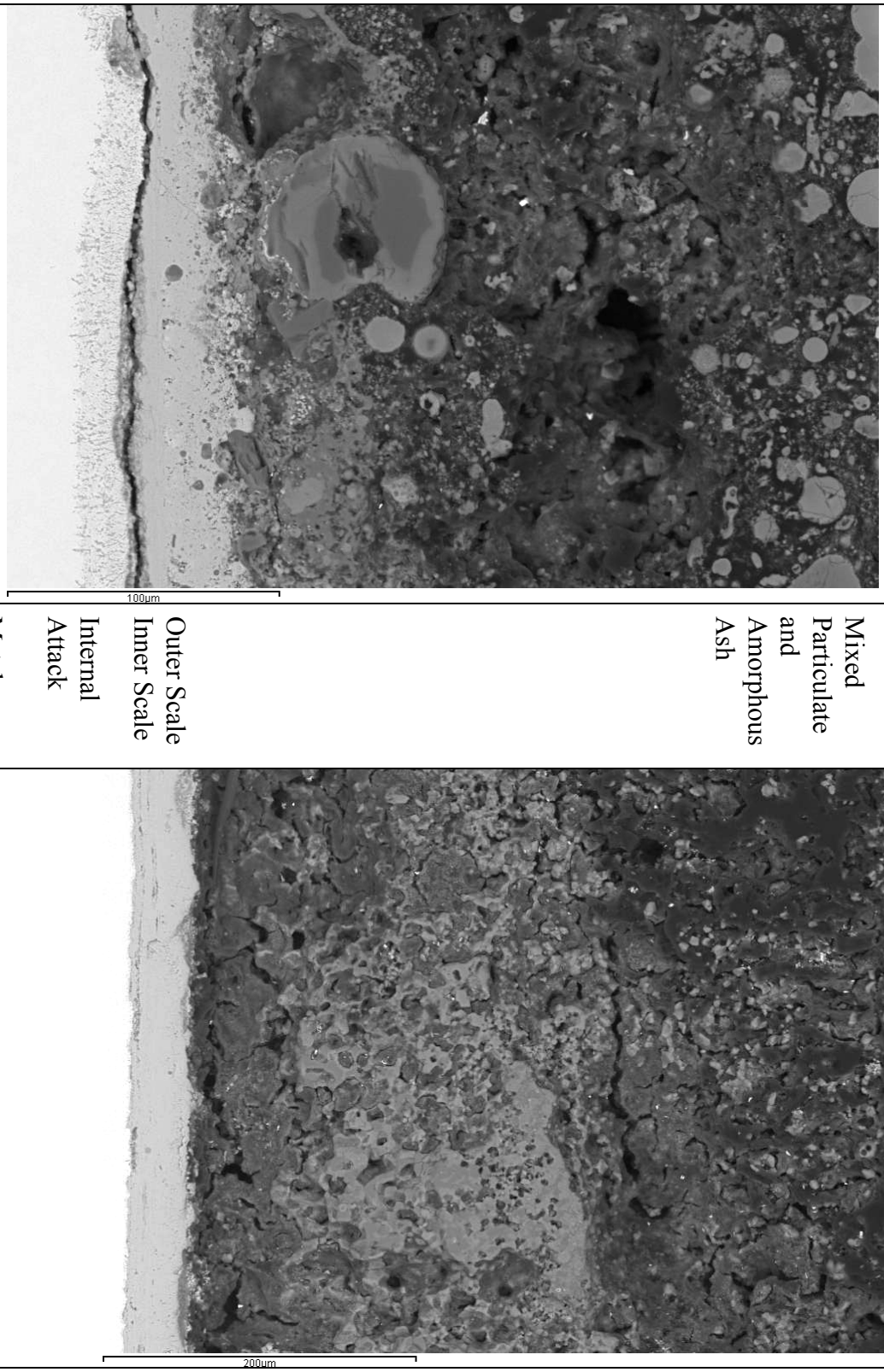

Figure 8: **SHTR96, SPECIMEN 5, T91, 571°C FOR 442 HOURS, ELECTRON IMAGES SHOWING IRREGULAR GENERAL AND SUBSURFACE ATTACK WITH DUPLEX CORROSION SCALES. SCALE OVERLAID BY MIXED A PARTICULATE AND AMORPHOUS ASH DEPOSIT**

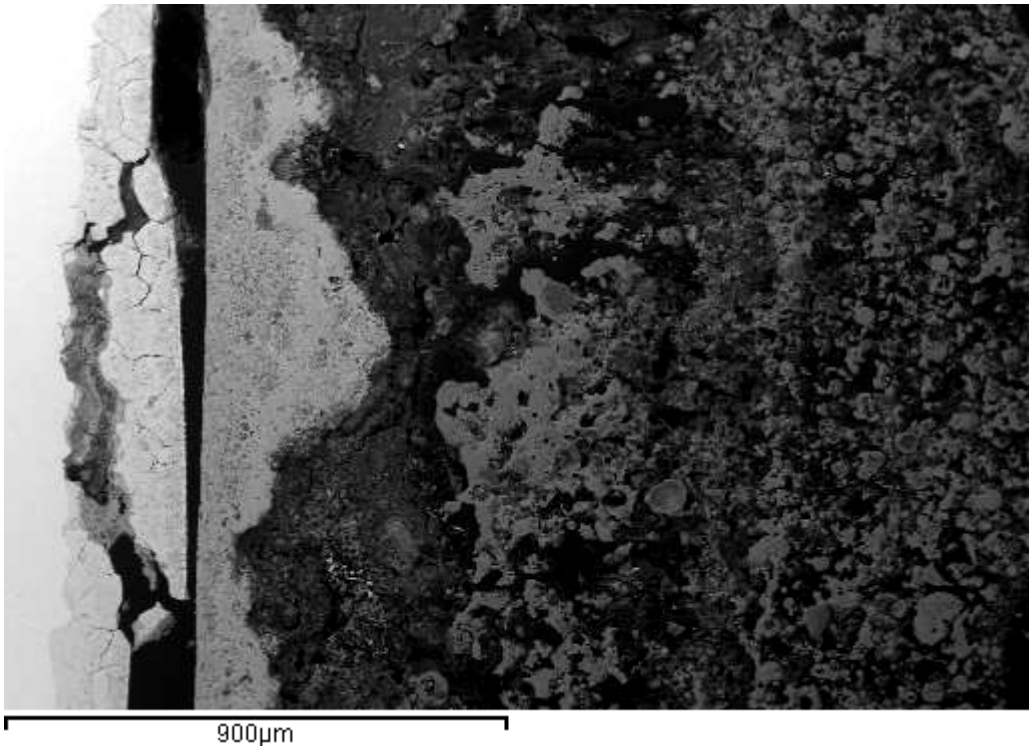

Figure 9: **SHTR96, SPECIMEN 8, SANICRO25, 608°C FOR 442 HOURS, LOW MAGNIFICATION BACK SCATTER ELECTRON IMAGE SHOWING GRAIN BOUNDARY AND SUBSURFACE ATTACK LEADING TO EXFOLIATION OF METAL GRAINS, FORMATION OF A DARK PHASE INTERNAL (SUB-SURFACE) SCALE AND OUTER SCALE. SCALE OVERLAID BY MIXED A PARTICULATE AND AMORPHOUS ASH DEPOSIT**

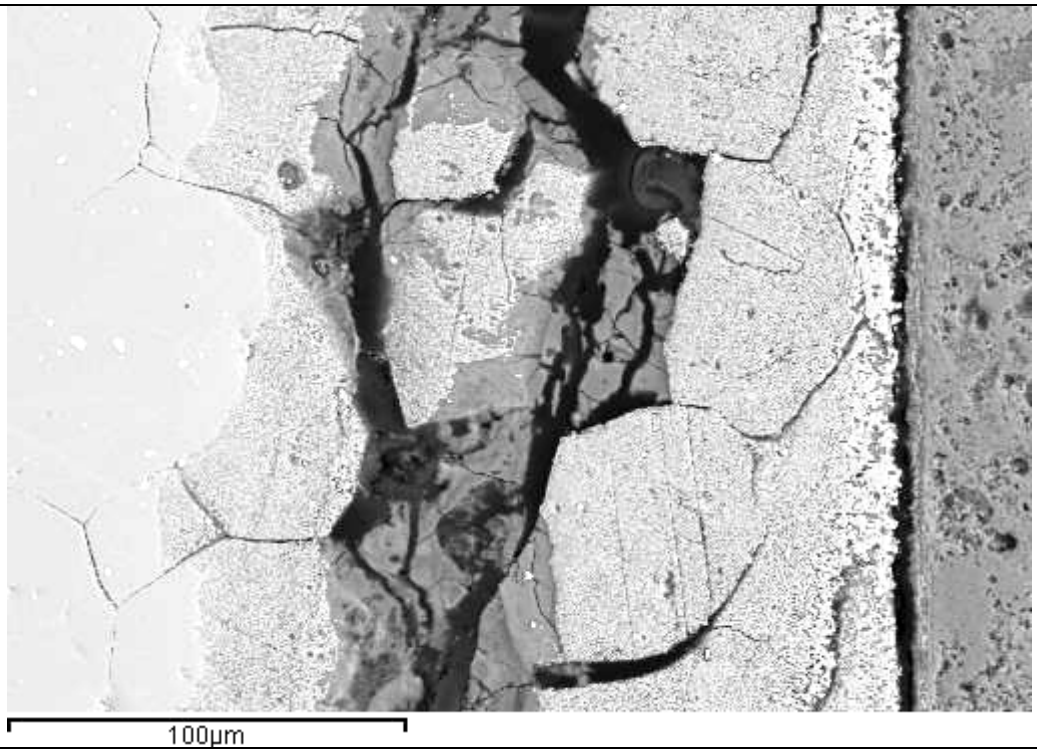

Figure 10: **SHTR96, SPECIMEN 8, SANICRO25, 608°C FOR 442 HOURS, HIGH MAGNIFICATION BACK SCATTER ELECTRON IMAGES SHOWING GRAIN BOUNDARY AND SUBSURFACE ATTACK LEADING TO EXFOLIATION OF METAL GRAINS, FORMATION OF A DARK PHASE INTERNAL (SUB-SURFACE) SCALE AND OUTER SCALE.**

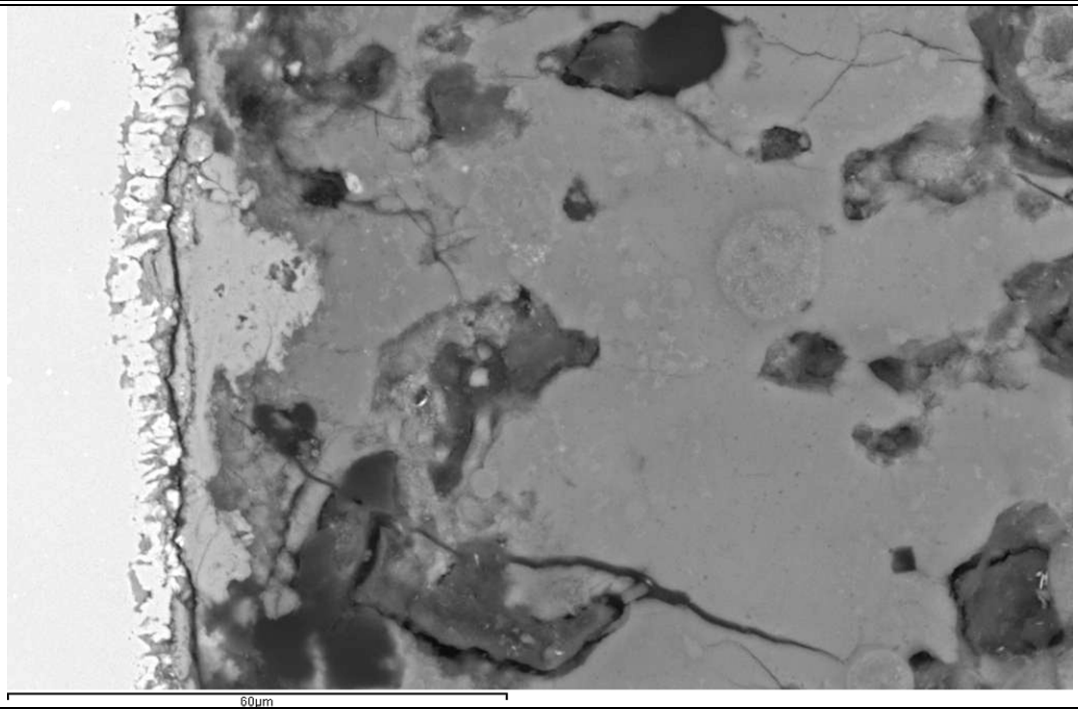

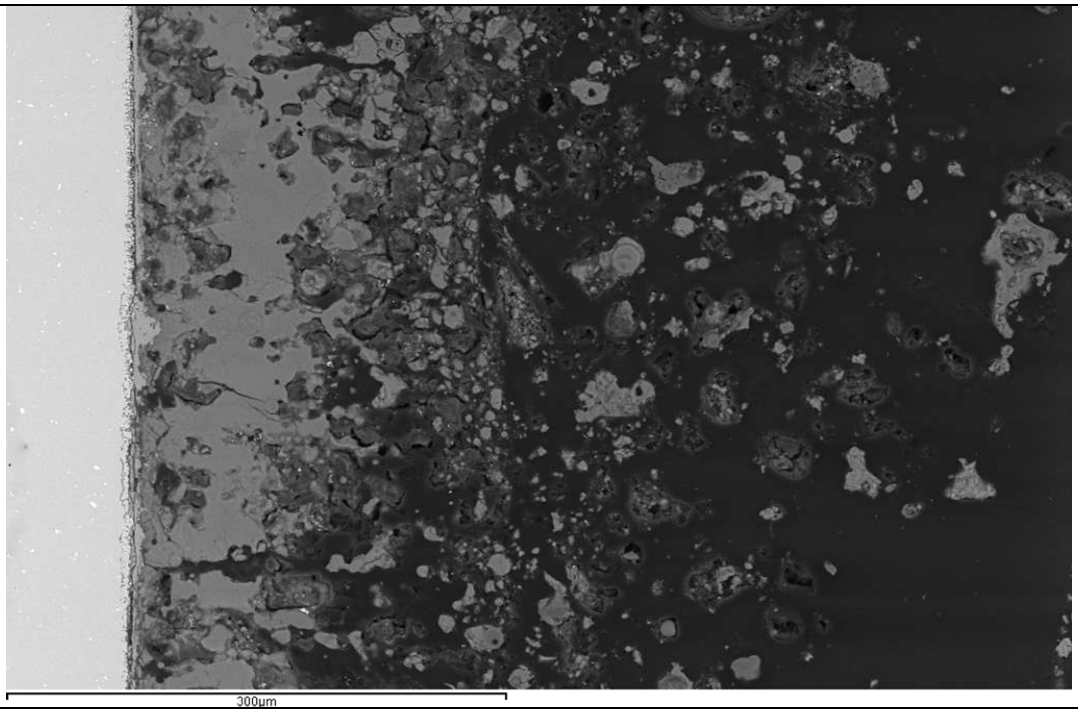

Figure 11: **SHTR96, SPECIMEN 9, TP347HFG, 619°C FOR 442 HOURS, BACK SCATTER ELECTRON IMAGES LOCALISED AND SUBSURFACE ATTACK LEADING TO THE FORMATION OF DUPLEX SCALES. SCALE OVERLAID BY MIXED A PARTICULATE AND AMORPHOUS ASH DEPOSIT**

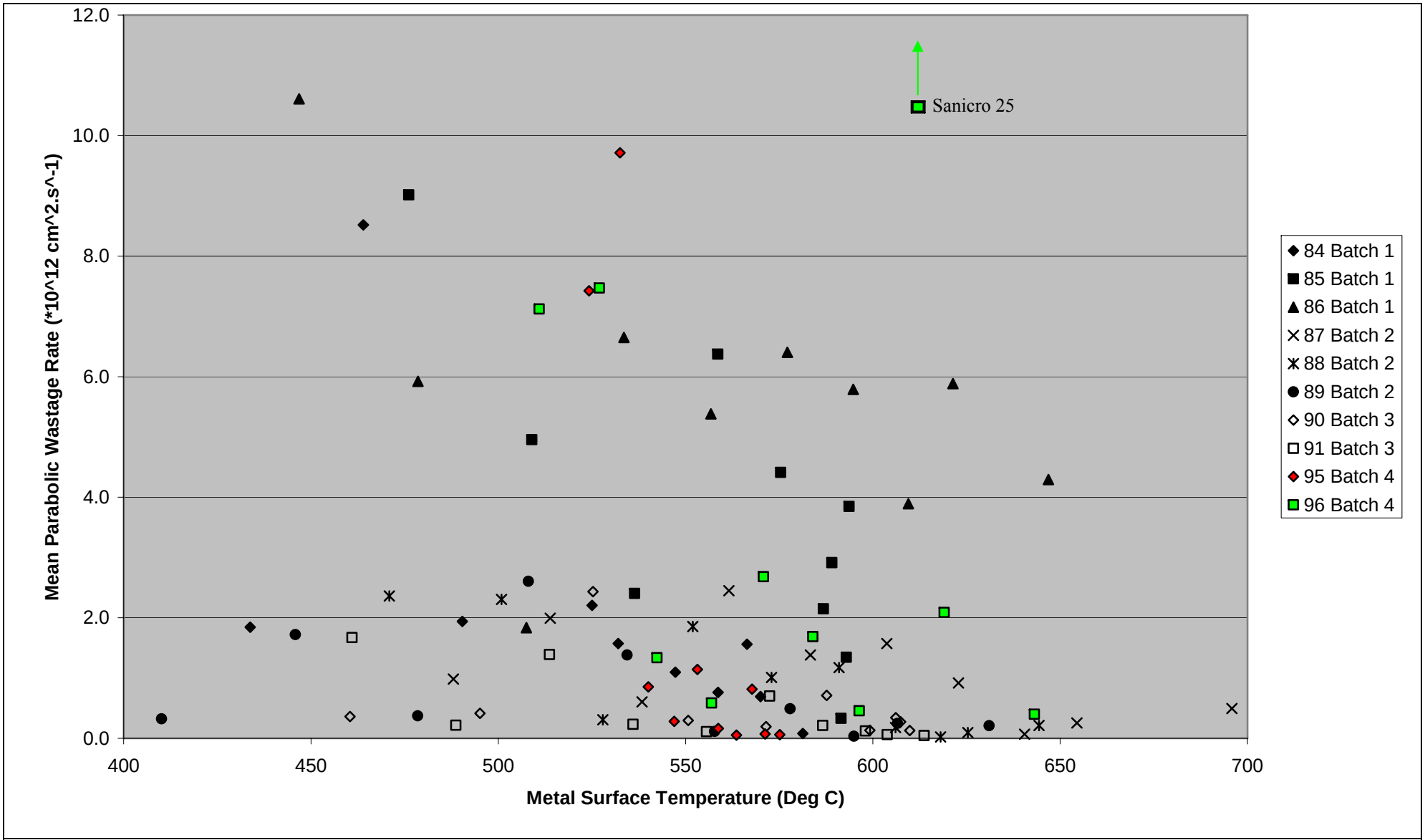

Figure 12: COMPARISON OF WASTAGE RATES FROM AMAGER (95 & 96) AND AVEDØRE CORROSION PROBES (84 – 91)

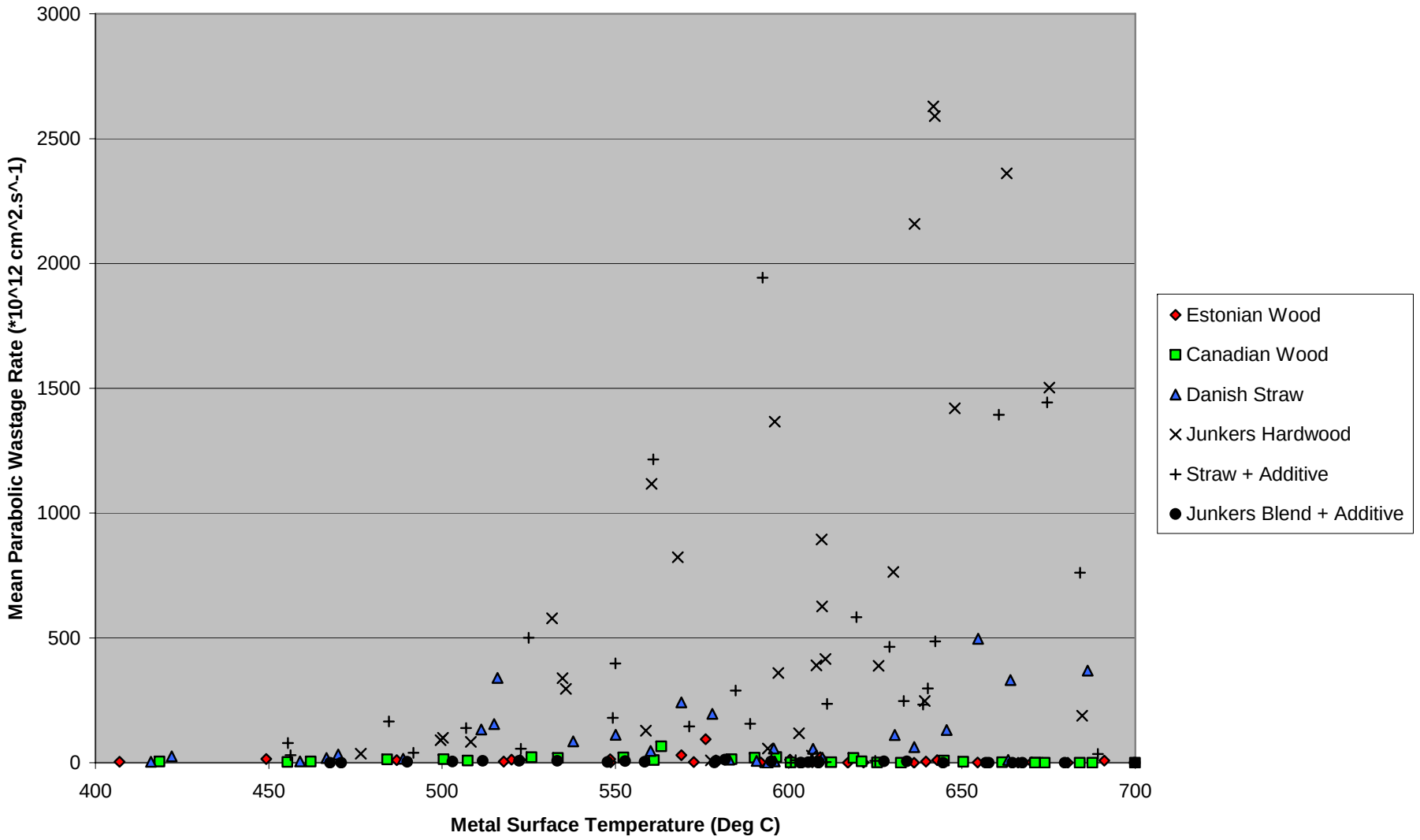

Figure 13: WASTAGE RATES MEASURED AFTER SHORT TERM (approx. 50 hours) PILOT SCALE TESTING